Design Effects of the Junction Contour of a Blended Rolled Edge Compact Range Reflector

M. Dirix [1], S.F. Gregson [2, 3]
[1] Antenna Systems. Solutions, Santander, Spain; mdirix@asysol.com
[2] Next Phase Measurements LLC, CA, USA
[3] Queen Mary University London, London, UK

***Abstract*—This paper is an extension of the authors prior work examining the design and optimisation of blended rolled edge (BRE) compact antenna test ranges (CATR) using evolutionary algorithms. The authors existing approach was initially improved and extended to provide broadband optimization of blended rolled edge (BRE) CATRs including refining the algorithm to take account of and reducing chamber wall illumination which is a recognized deficiency of the BRE CATR approach. In this paper the design approach is further extended to include the junction contour which in this study is adapted to remove the discontinuity in the reflector surface that is typically present in BRE CATRs, and further increases the available CATR design envelope. Worthwhile improvements in predicted QZ performance are obtained together with a further reduction in chamber wall illumination. These are highlighted together with the important reduction in the BRE reflector volume and mass.**

Index Terms— CATR, antenna measurement, blended rolled edge, genetic optimisation, superformula, junction contour, 5G.

I. INTRODUCTION

The concept of a blended rolled edge reflector for use with a compact antenna test range (CATR) was first proposed by Burnside and reported in the open literature in [1]. This concept used a smooth transition from the central parabolic portion of the reflector, which collimates the illuminating field to produce the pseudo plane wave which propagates to the quiet-zone (QZ), to the elliptically curved surface which progressively directs the energy away from the QZ and terminates the reflector edge. In this original work, and indeed in much that has followed, the description of the reflector surface profile was expressed in a parametric form of azimuthal angle, and radial distance [1]. This provided a convenient way in which to describe the three distinct portions of the reflector: the parabolic portion, the blended portion, and the elliptically curved edge portion, with the transition between them being specified in terms of a radial distance r, where r is a function of the azimuthal angle ϕ. In three dimensions, this corresponds to a single closed Junction Contour (JC). The blending from one region to another must be completely smooth to ensure that no diffraction occurs at the boundary and that the surface currents flow freely. The merits of a blended rolled edge (BRE) approach have been widely discussed in the open literature [1], [2], [3] however the benefits are usually not as great as is suggested by computational electromagnetic (CEM) simulations as these predictions, and simulated QZ measurements, mostly neglect to account for the increased wall reflections resulting from the redirected energy from the blended rolled edge, and which is failed to be effectively absorbed by the anechoic chamber lining and which subsequently enters the CATR QZ thereby degrading the quality of the collimated pseudo plane-wave.

While both industry and academia have been largely focussed on performing the optimisation of the BRE reflector surface curvature by examining the mechanical properties of the reflector curvature, where continuity of the curvature at the junction between the parabolic section and the elliptical section is typically examined, it is crucial to recognise that ultimately, it is the quality of the pseudo plane wave that is of paramount importance to the performance of the CATR. It is also important to note that, inherently, the parabolic and elliptical curvatures have opposing derivative signs. We must match not only the surface profile function, but as many of its derivatives as possible, across the entire reflector surface, to be able to minimise unwanted diffraction effects. Here however, there is a problem. The junction contour is a primary driver for the final reflector's cross-sectional shape. Thus, the classical design of the junction contour has largely been formulated and specified to produce a generally square, or rectangular, cross sectional shape for the reflector profile. However, as a result of the mathematical form of the JC, this necessitates it taking on the form of an astroid, *i.e.* a tetracuspid shape that is reminiscent of a concave sided square (or rectangle), exhibiting cusps in each of the four corners. This form of JC introduces undesirable "creases" in the realised reflector surface that can be seen in many BRE CATR implementations that follow this approach. As these sorts of discontinuity can form sources of unwanted diffraction, this is clearly at odds with the desire for a smoothly curving, blended, surface profile which is at the very heart of this design concept. In this paper we show how this problem can be addressed, and highlight the additional degrees of freedom that the new approach can provide and the ways in which this can be harnessed to further improve the performance of BRE CATRs.

As noted above, and as was shown in [4], [5] and [6], in order to further improve the BRE reflector design the optimization of the reflector curvature must be driven by the quiet zone (QZ) performance rather than purely by the continuity of the reflector surface. The QZ orientated approach utilised a powerful and efficient genetic optimisation strategy that incorporates a fast, parallel,

implementation of the necessary electromagnetic field propagation and which has been shown to be capable of breeding high performance BRE CATRs [6]. The genetic optimisation approach is one that is ideally suited to tackling many variable optimisation problems which, as we shall show below, can be easily extended to consider the ideal form for the JC. Thus, the next section sets out the method for parameterising the JC before progressing to show the results of a series of optimisations which demonstrate the improvements in QZ performance and increased flexibility of range design. The paper concludes by presenting a summary and the plans for the future work.

II. Expression of the Junction Contour

As was expounded within the previous section, the JC is perhaps the main driver for the final reflector shape. The enclosed surface defines the region where the reflector has a parabolic shape, and thus determines directly the overall shape and size of the CATR QZ. The curvature of each portion of the reflector, whether concave or convex determines the outline shape of the reflector itself. While the junction contour is a crucial factor in the determination of the final overall shape of the BRE reflector, surprisingly little attention has been paid to its form in the open literature, with virtually no changes being made to its original definition, *cf.* [1], [2] and [3]. It is noted here though, that in [6], the original definition was expanded to admit rectangular shaped reflectors that in its final form, can be expressed as:

$$x_j' = \begin{cases} R_{QZ,x} + r_{e,h}(1-\cos\varphi') & 0 \le \varphi' \le \varphi_1 \\ (R_{QZ,y} + r_{e,v})\cot\varphi' - r_{e,h}\cos\varphi' & \varphi_1 \le \varphi' \le \varphi_2 \\ -R_{QZ,x} - r_{e,h}(1+\cos\varphi') & \varphi_2 \le \varphi' \le \varphi_3, \\ -(R_{QZ,y} + r_{e,v})\cot\varphi' - r_{e,h}\cos\varphi' & \varphi_3 \le \varphi' \le \varphi_4 \\ R_{QZ,x} + r_{e,h}(1-\cos\varphi') & \varphi_4 \le \varphi' \le 2\pi \end{cases} \quad (1)$$

$$y_j' = \begin{cases} (R_{QZ,x} + r_{e,h})\tan\varphi' - r_{e,v}\sin\varphi' & 0 \le \varphi' \le \varphi_1 \\ R_{QZ,y} + r_{e,v}(1-\cos\varphi') & \varphi_1 \le \varphi' \le \varphi_2 \\ -(R_{QZ,x} + r_{e,h})\tan\varphi' - r_{e,v}\sin\varphi' & \varphi_2 \le \varphi' \le \varphi_3, \\ R_{QZ,y} - r_{e,v}(1+\cos\varphi') & \varphi_3 \le \varphi' \le \varphi_4 \\ (R_{QZ,x} + r_{e,h})\tan\varphi' - r_{e,v}\sin\varphi' & \varphi_4 \le \varphi' \le 2\pi \end{cases} \quad (2)$$

with,

$$\varphi_1 = \tan^{-1}\left(\frac{R_{QZ,y}+r_{e,v}}{R_{QZ,x}+r_{e,h}}\right), \quad (3)$$

$$\varphi_2 = \pi + \tan^{-1}\left(\frac{R_{QZ,y}+r_{e,h}}{-R_{QZ,x}-r_{e,v}}\right), \quad (4)$$

$$\varphi_3 = \pi + \tan^{-1}\left(\frac{-R_{QZ,y}-r_{e,h}}{-R_{QZ,x}-r_{e,v}}\right), \quad (5)$$

$$\varphi_4 = 2\pi + \tan^{-1}\left(\frac{-R_{QZ,y}-r_{e,h}}{R_{QZ,x}+r_{e,v}}\right), \quad (6)$$

and $r_{e,h}, r_{e,v}$ are the junction contour curve parameters in the horizontal and vertical direction respectively, and $R_{QZ,x}, R_{QZ,y}$ is the radius of the QZ in x and y directions. Evidentially, from the piecewise form of the definition of the current JC formulation, a discontinuity is formed in the corners at $\varphi_1, \varphi_2, \varphi_3$ and φ_4 where a series of cusps are introduced. This discontinuity leads to the astroid form of the JC and the discontinuity in the derivative of the reflector surface profile, which can be observed in many realised BRE CATR reflectors [7]. In order to remove the surface discontinuity an alternative junction contour definition is required which must have continuous first and second derivatives, *i.e.* is a smoothly varying continuous function everywhere, in the corners, while still allowing the required degree of flexibility for the contour to shape the reflector as required by (1) and (2). It can be seen that the SuperFormula [8] is of a suitable form that is amenable to these requirements, and when defined in polar coordinates can be expressed as,

$$r(\varphi) = \left(\left|\frac{1}{a}\cos\left(\frac{m}{4}\varphi\right)\right|^{n_2} + \left|\frac{1}{b}\cos\left(\frac{m}{4}\varphi\right)\right|^{n_3}\right)^{-\frac{1}{n_1}} \quad (7)$$

where m describes the number of rotational symmetries, a, b are amplitude factors, and n_1, n_2 and n_3 determine the radial shape. By way of an illustration, in Fig 1. a comparison is shown between the standard piecewise defined JC, and an equivalent SuperFormula based JC. In this particular case $m = 4$ and n_1, n_2 and n_3 where chosen such that the curvature matches closely the shape of the original JC. Crucially, and as was expounded above, from inspection of Fig. 1, it can be seen that the SuperFormula shows no discontinuities in the corners, thereby insuring the BRE reflector surface profile is also smooth. However, during the optimisation that is presented within the following section, the shape of the junction contour is also permitted to vary as part of the optimisation as this results in an further increase in the degrees of freedom available for shaping the reflector and improving the CATR QZ performance.

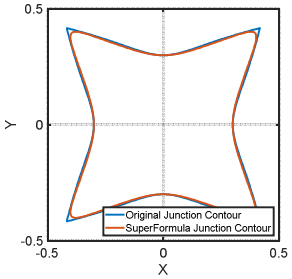

Fig. 1. Comparison of the original junction contour and the approximating, smooth, equivalent, SuperFormula contour.

III. CATR Simulations

A BRE [6] CATR was optimized using the simulation technique developed in [7] and validated in [6], [9], with the evolutionary optimisation strategy presented previously within [4], [5], and using the CATR configuration described in [6]. Here, a population of 100 individual reflector profiles were created at random, with these spanning the complete design space whose domain was bounded by certain predefined geometrical constraints. The "optimal" six designs, as determined by evaluation of the quality of the pseudo plane wave within the CATR QZ [7], were taken and subsequently used as parents to breed a new generation of 24 parameter permuted and mixed descendants [4]. This process was then repeated until the termination condition was reached,

with this being predicated on either minimal variation of the penalty function between generations, or a maximum runtime of 400 generations being reached. This was performed for the case where the superformula (SF) based JC was employed while maintaining the maximum dimensions of the reflector and the nominal size of the parabolic portion of the reflector so as to make the comparison as consistent as possible. The respective reflector shapes can be seen presented below in Fig. 2, with a comparison of the corners of the reflectors being shown in Fig. 3 which highlights the removal of the corner "crease" in the SF based JC design which has been highlighted here by the red ellipse. Although the exterior shape has changed, the overall width and height of the reflector is unchanged, as too is the width and height of the parabolic portion of the reflector.

Fig. 2. BRE CATR reflector with standard JC (left) and equivalent SF based JC (right).

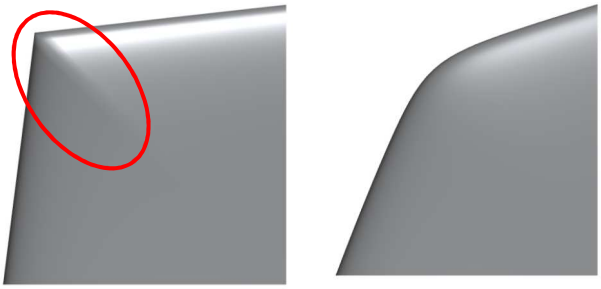

Fig. 3. Corner of BRE reflector showing classical JC induced crease (left) hilighted by red ellipse, versus SF based JC corner without crease shown (right).

From inspection of these plots we see that the SF JC yields a more rounded form to the QZ field distributions. This can be seen in both Fig. 4 and Fig. 5 which are respectively the copolar amplitude and phases of the pseudo plane-wave in the QZ. In Fig. 6 we can also see that the level of the Cross-Pol. has been reduced and overall a better control. This subtle change in form is however not an issue when testing antennas using a conventional ϕ over θ "model tower" spherical positioner as the AUT aperture traces out a circular cross-sectional portion of the QZ. That is to say, the "corners" of the "squarer" QZ are not typically coupled to the fields of the AUT, unless that is, one happens to be testing a square antenna with corners protruding outside the circular limits of the QZ (as denoted by the dotted blue line in Fig. 4) using an azimuth stage taking purely azimuth great circle cuts and is the limiting case where the AUT occupies nearly all of the cross-section of the pseudo plane wave.

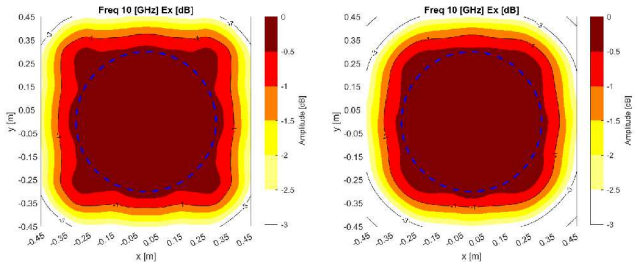

Fig. 4. Copolar amplitude classical JC (left) and SF based JC (right).

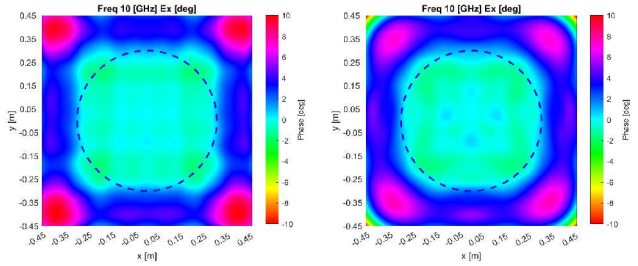

Fig. 5. Copolar phase classical JC (left) and SF based JC (right)

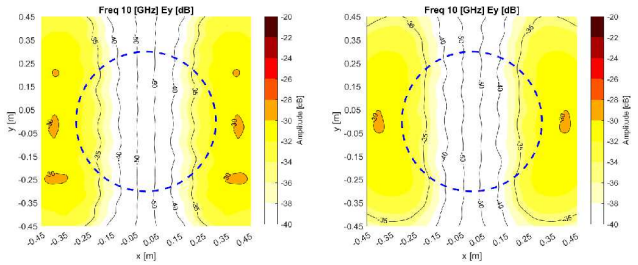

Fig. 6. Cross-polar amplitude classical JC (left) and SF based JC (right).

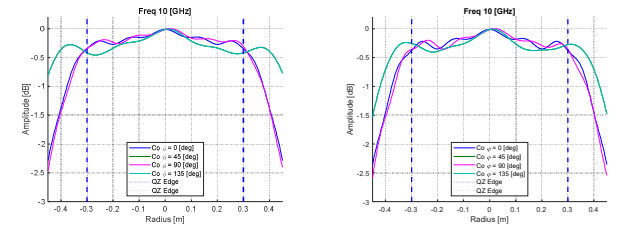

Fig. 7. Copolar amplitude cuts classical JC (left) and SF based JC (right).

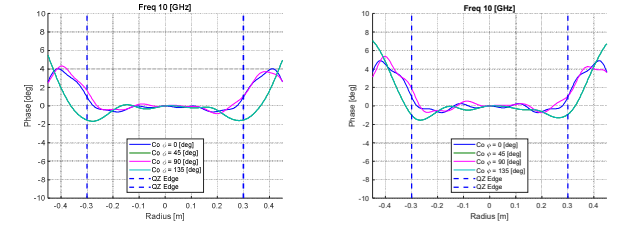

Fig. 8. Copolar phase cuts classical JC (left) and SF based JC (right).

The change in JC definition also provides an enhanced ability to control the QZ field in the inter-cardinal, *e.g.* 45° region. We can see this effect in Fig. 7 and 8 where we observe an improvement in the uniformity of the amplitude and phase cuts. As a further illustration, Table I below presents a comparison of the amplitude taper, amplitude ripple and phase total variation QZ parameters for the horizontal,

vertical and 45° cuts for both the classical JC, and SF based JC CATRs.

TABLE I. BRE CATR QZ PERFORMANCE METRICS

Angle of Cut [deg]	Performance at 10 GHz		
	CATR QZ Parameter	*Standard*	*With SF*
0	Amplitude Taper	0.23 dB	0.24 dB
0	Amplitude Ripple	0.16 dB	0.23 dB
0	Phase Total Variation	1.58 deg	1.64 deg
45	Amplitude Taper	0.42 dB	0.25 dB
45	Amplitude Ripple	0.20 dB	0.30 dB
45	Phase Total Variation	1.78 deg	1.56 deg
90	Amplitude Taper	0.24 dB	0.26 dB
90	Amplitude Ripple	0.17 dB	0.27 dB
90	Phase Total Variation	2.46 deg	2.61 deg

As expected, from inspection of Table I we see that the performance of the classical and modified CATR QZ performances are very similar for the horizontal and vertical cuts. However, for the inter-cardinal 45° cut the SF based JC has a benefit in terms of performance over the baseline classical design in terms of amplitude taper and phase total variation. Thus in summary, from inspection of the 2D false-colour checker-board plots pattern the SF based JC QZ performance can be seen to be very much smoother than the baseline JC alternative. This is a pleasing result. The design philosophy of the BRE CATR was predicated upon the desire that the reflector surface be smooth as possible. As a minimum, the SF based JC has removed an undesirable artefact from the classical BRE CATR reflector design whilst preserving QZ performance, and in some areas yielded a worthwhile improvement. However, the additional degrees of freedom that use of the SF permit enable new, more general BRE CATR designs to be created with a slew of additional properties. This is the subject of the next section.

IV. GENERALISED SF CONTOUR CATR SIMULATIONS

As a further examination of the behaviour of the modified JC, the CATR reflector was re-optimised only this time the m variable which determines the degree of rotational symmetry was also permitted to vary. In the previous section, the CATR was optimised for the case of the SF JC. Then, the standard and SF based JCs were used to create two largely comparable reflectors, with all other parameters being held constant. Here however, the optimisation was run twice, once for the case where $m = 4$, and again when $m = 6$. Additionally, the n_2 and n_3 parameters were forced to be equal so as to insure horizontal and vertical symmetry in the final reflector profile and to accelerate the optimisation process, which was different from the optimisation that was performed in the previous section. The odd order m values were not included as these tend to yield reflectors with properties that diverge very significantly from those that we desire. The CATR QZ performance was then determined and can be seen presented in the following figures. The respective BRE CATR reflectors can be seen presented as rendered drawings in Fig. 9, $m = 4$ left, and $m = 6$ right.

Fig. 9. $m = 4$ (left) and $m = 6$ (right) blended rolled edge reflector profiles.

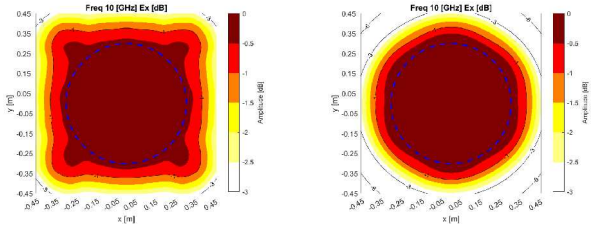

Fig. 10. Copolar amplitude $m = 4$ (left) and $m = 6$ (right).

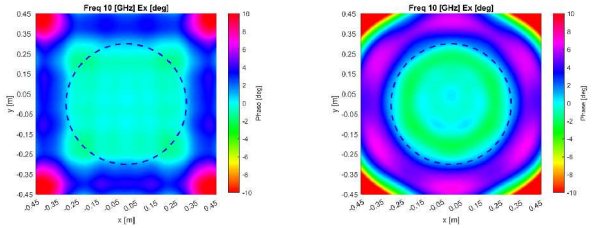

Fig. 11. Copolar phase $m = 4$ (left) and $m = 6$ (right).

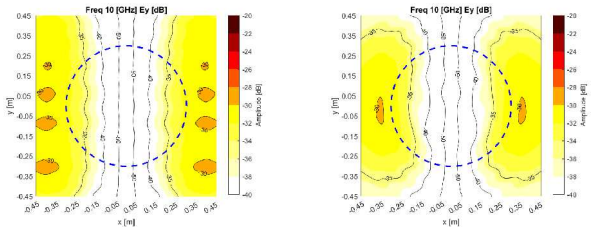

Fig. 12. Cross-polar amplitude $m = 4$ (left) and $m = 6$ (right).

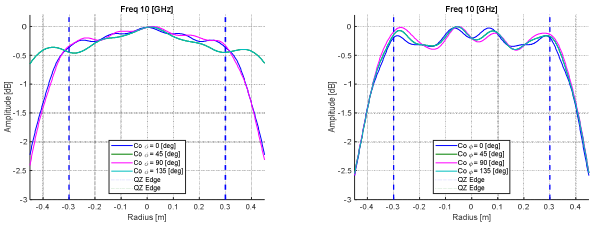

Fig. 13. Copolar amplitude cuts $m = 4$ (left) and $m = 6$ (right).

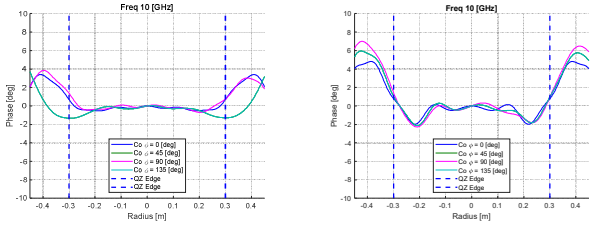

Fig. 14. Copolar phase cuts $m = 4$ (left) and $m = 6$ (right).

Here, the $m = 4$ SF JC tend to yield reflectors that are much more similar to the classical BRE CATR reflector designs. However, the greater rotational symmetry of the $m = 6$ SF JC

is evident from inspection of Fig. 9, with the effects of this characteristic being evident in the CATR QZ performance as illustrated in Fig = 10 to 14 inclusive. While the $m = 6$ design betters the $m = 4$ design in terms of amplitude taper, in all other respects its performance is subtly degraded. This can also be seen from inspection of table II below. However, this is perhaps a little misleading as the performances is very similar, and although the maximum width and height of the $m = 6$ reflector is the same as the $m = 4$ reflector, the $m = 6$ reflector is substantially *smaller* in terms of the amount of material, *e.g.* aluminium, that is used within its construction, allow a weight reduction of approximately 28 %. This is very beneficial in terms of manufacture, installation and shipping.

TABLE II. BRE CATR QZ PERFORMANCE METRICS

Angle of Cut [deg]	**Performance at 10 GHz**		
	CATR QZ Parameter	***M = 4***	***M = 6***
0	Amplitude Taper	0.27	0.13
0	Amplitude Ripple	0.12	0.29
0	Phase Total Variation	1.20	2.74
45	Amplitude Taper	0.45	0.06
45	Amplitude Ripple	0.14	0.37
45	Phase Total Variation	1.38	3.13
90	Amplitude Taper	0.27	0.11
90	Amplitude Ripple	0.14	0.42
90	Phase Total Variation	2.04	3.66

However, there is a further very valuable benefit of the rounder $m = 6$ reflector design and that is in terms of the way it redirects radiation within the housing anechoic chamber. Fig. 15 presents the fields reflected from the respective CATR reflectors at 10 GHz that illuminate the walls of an enclosing anechoic chamber that is 1500 × 1500 × 3000 mm [H × W × L], *cf.* [5]. Here, the feed illumination, tilt angle, *etc*. are consistent between the respective configurations to insure the comparison is as direct as is possible. In each of these examples, the CATR is floor fed with the circular horn feed being tilted up in elevation so that the boresight direction is orientated to point a little beyond the geometrical centre of the reflector so as to best equalize the amplitude taper within the CATR QZ. The wall illuminations shown in Fig. 15 are computed from the field *reflected* by the CATR reflector, *i.e.* the direct feed illumination is not included here. This clearly illustrates where the greatest field intensities illuminate the chamber walls, and these can be used to aid in the design of the chamber absorber. Crucially, the additional flexibility in the specification of the junction contour has provided a CATR design that has lower levels of wall illumination than the corresponding traditional approach, and significantly lower intensities in middle of the sides, ceiling and floor, which is known to adversely affect the quality of measurements made in these cuts, *i.e.* azimuth or elevation.

V. SUMMARY, CONCLUSIONS & FUTURE WORK

In this work it was shown that a replacement of the JC by a rotationally continuous function improves the smoothness of the BRE reflector profile. This improved smoothness provides an improvement mostly seen in the intercardinal cuts of the QZ performance. The proposed replacement of the JC by the SF generated JC has been shown to provide additional degrees of freedom allowing the employed optimization technique to further shape the reflector. Among others, increased rotational symmetries allow for a non-square reflector shape which distributes the diverted power from the reflector edges more evenly over the chamber walls, as opposed to a concentration on the specular areas which are expected to propagate directly to the QZ. A further important aspect which is being research is the required length of the backfolded edge of the BRE reflector. Depending on this requirement the reflector thickness and thus its overall weight can be further optimised.

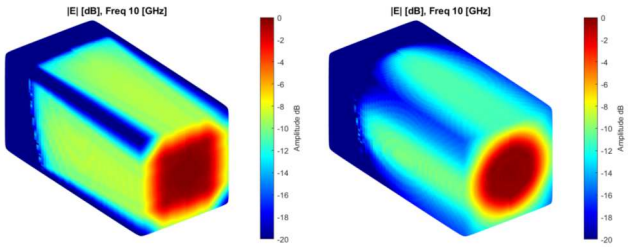

Fig. 15. Installed classical JC serrated (left) and blended rolled edge (right) reflector

REFERENCES

[1] W. Burnside, M. Gilreath, B. Kent en G. Clerici, „Curved Edge Modification of Compact Range Reflector," *Antennas and Propagation, IEEE Transactions on,* vol. 35, nr. 2, pp. 176-182, 1987.

[2] I. Gupta and W. Burnside, "A Method to Design Blended Rolled Edges for Compact Range Reflectors," The Ohio State University, ElectroScience Laboratory, Columbus, 1989.

[3] I. Gupta, K. Ericksen en W. Burnside, „A Method to Design Blended Rolled Edges for Compact Range Reflectors," *Antennas and Propagation, IEEE Transactions on,* vol. 39, nr. 6, pp. 853-861, 1990.

[4] M. Dirix, S. Gregson and R. Dubrovka, "Genetic Evolution of the Reflector Edge Treatment of a Single Offset-Fed Compact Antenna Test Range for 5G New Radio Applications," in *AMTA Annual Meeting and Symposium*, Daytona Beach, Florida, 2021.

[5] M. Dirix, S. Gregson and R. Dubrovka, "Genetic Optimization of Edge Treatmens of Single Offset Reflector Compact Antenna Test Ranges," in *AMTA Annual Meeting and Symposium*, Denver, CO, 2022.

[6] S. Gregson, M. Dirix and R. Dubrovka, "Efficient Optimization of the Blended Rolled Edge of a Rectangular Single Offset Fed Compact Antenna Test Range Reflector Using Genetic Evoluation," in *EuCAP*, Madrid, 2022.

[7] C. Parini, S. Gregson, J. McCormick, D. Janse van Rensburg en T. Eibert, Theory and Practice of Modern Antenna Range Measurements, 2nd Expanded Edition, IET Press, 2021.

[8] J. Gielis, Inventing the Circle, Antwerpen: Geniaal bvba, 2003.

[9] R. Dubvrovka, C. Parini and S. Gregson, "Validation of Blended Rolled Edge Reflector Characteristics for Compact Test Ranges," in *European Conference on Antennas and Propagation (EuCAP)*, Florence, Italy, 2023.

[10] M. Dirix and S. Gregson, "Optimization of the Serration Outline Shape of a Single Offset Fed Compacte Antenna Test Range Reflector," in *EuCAP*, Düsseldorf, 2021.